Temporal Changes of Subsurface Velocities during Strong Shaking as Seen from Seismic Interferometry

Masumi Yamada

Pioneering Research Unit for Next Generation, Kyoto University, Uji, Gokasho, 611-0011, Japan

Jim Mori

Disaster Prevention Research Institute, Kyoto University, Uji, Gokasho, 611-0011, Japan

Shiro Ohmi

Disaster Prevention Research Institute, Kyoto University, Uji, Gokasho, 611-0011, Japan

Abstract. We apply a deconvolution method to a strong motion dataset recorded at the surface and in boreholes in northeast Honshu, Japan. We try to characterize the non-linear effects of the subsurface soil during strong shaking and show the change of the subsurface velocity structure during the shaking.

The deconvolved waveforms reflect the subsurface velocity structure, and their horizontal and vertical components correspond to S- and P-wave, respectively, traveling from the borehole to the ground surface. The strong motion records with smaller values of peak acceleration do not include significant non-linear effects, so the deconvolved waveforms of the observed accelerations can be well simulated by the program SHAKE91.

For high acceleration motions during the shaking of two separate earthquakes, large reductions of near-surface velocities are seen. In results for the 2008 Iwate-Miyagi Nairiku earthquake, the large high-frequency ground motions over 4g at one near-source station, caused a non-linear response of the soil, and the reduction of the average shear wave velocity reached 24%. This corresponds to a stiffness change of over 75%. The soil properties and the stiffness coefficient which changed during the shaking did not fully recover after the shaking, leaving a static change.

1. Introduction

Cross correlations can be used to extract response functions from multiple sets of similar waveforms. The cross-correlation of the waves recorded at a receiver gives the superposition of the delayed and advanced Green's function, if noise sources are uniformly distributed on all sides of the receivers [Snieder, 2004, @]. This technique has recently been applied in many seismic studies and various study areas [e.g. Sabra et al., 2005, @; Mehta et al., 2007, @; Brenguier et al., 2008, @; Vasconcelos and Snieder, 2008a, @; Vasconcelos and Snieder, 2008b, @].

Most past results use ambient noise data and average the data over sufficiently long periods so that the assumption that the sources become uniformly distributed is valid. However, using the deconvolution of two sets of waveforms recovers the impulse response between two receivers without the need for an independent estimate of the source function [Vasconcelos and Snieder, 2008b, @]. For example, Snieder and Safak, 2006 [@] extracted the building response from the excitation and ground coupling by deconvolving the motion recorded at the different levels of a multi-floor building. Kohler et al., 2007 [@] computed the impulse response functions of a moment-frame building by deconvolution, and Miyazawa et al., 2008 [@] extracted downward propagating P- and S-waves from industrial noise in a borehole array.

We apply this deconvolution technique to strong motion data with a set of ground surface and borehole accelerograms in northeast Honshu, Japan. Here, we focus mainly on the 2008 Iwate-Miyagi Nairiku earthquake (M_w 6.9, M_{jma} 7.2), which occurred in southwest Iwate prefecture (39.03°N, 140.88°E, depth 8 km) on June 14, 2008 at 23:43:45 GMT. This earthquake produced high-frequency ground motions, which resulted in large values of PGA (peak ground acceleration). Station IWTH25 of KiK-net (Kiban-Kyoshin Network operated by the National Research Institute for Earth Science and Disaster Prevention) located 3 km southwest of the epicenter, recorded a very large PGA (4278 cm/s^2 for the vector sum of the three components). In general, a large excitation causes non-linearization of the subsurface soil and the shear-wave velocity relaxation following to the velocity reduction during shaking [Arai, 2006, @; Brenguier et al., 2008, @]. In this paper, we try to characterize the nonlinear effects of the subsurface soil during strong shaking and the static change of the subsurface velocity structure using deconvolved waveforms of KiK-net data.

2. Strong Motion Data

Near-field ground motions of the 2008 Iwate-Miyagi Nairiku earthquake along with aftershocks and other small events, were recorded on KiK-net. These stations cover all of Japan and the data can be downloaded from their website [KiK-net, 2000, @]. The advantage of this network is that all stations have a borehole of 100 m or more in depth and accelerographs have been installed both on the ground surface and at the bottom of boreholes. The site information measured in the boreholes includes soil type with P- and S-wave velocity profiles. Three-component accelerograms are recorded with a maximum of 4000 cm/s^2. The sampling interval is 100 Hz after November 2007 and 200 Hz before then.

In this analysis, we use records at 14 stations within 50 km of the epicenter of the 2008 Iwate-Miyagi Nairiku earthquake (see Figure 1). The number of smaller earthquake

0148-0227/09/$9.00

records varies with the station, but the average number of well recorded M_w 3.0 to M_w 6.9 events at a single station is 314. The recording period is from January 2000 to December 2008.

3. Method

3.1. Deconvolution Method

We use a deconvolution method to extract the subsurface soil response [Snieder and Safak, 2006, @]. For each event at each station, the acceleration waveform at the ground surface is deconvolved by the acceleration waveform recorded at the bottom of the borehole. The acceleration at the ground surface and bottom of the borehole in the frequency domain are $U_1(\omega)$ and $U_2(\omega)$, respectively, and the transfer function $G(\omega)$ is given by;

$$G(\omega) = \frac{U_1(\omega)U_2^*(\omega)}{U_2(\omega)U_2^*(\omega)}. \quad (1)$$

where the asterisk denotes the complex conjugate. Note that the numerator in equation 1 is the cross correlation in frequency domain of the acceleration at the ground surface with the bottom of the borehole, and the denominator is the power spectrum of the acceleration at the bottom of the borehole. To avoid instability problems due to spectral minima in the denominator, we used a 10% water-level correction [Clayton and Wiggins, 1976, @].

$$G(\omega) = \frac{U_1(\omega)U_2^*(\omega)}{|U_2'(\omega)|^2}, \quad (2)$$

where

$$|U_2'(\omega)|^2 = \begin{cases} |U_2(\omega)|^2 & \text{if } |U_2(\omega)| \geq 0.1 \max|U_2(\omega)| \\ 0.1 \max|U_2(\omega)|^2 & \text{if } |U_2(\omega)| < 0.1 \max|U_2(\omega)|. \end{cases} \quad (3)$$

$G(\omega)$ is transformed back to the time domain, $g(t)$. The physical meaning of $g(t)$ with $t > 0$ is a wave that propagates upward direction. The delay from time zero shows the travel time from the downhole sensor to the surface.

In the problem of the traveling wave from the subsurface to the ground surface, the function $g(t)$ includes the wave propagating upward to the ground surface, and the reflected wave traveling downward. Figure 2 (left) shows an example for an input delta function at the bottom of a borehole in a half space. The impulse wave travels to the surface, and reflects back downward. Therefore, the acceleration recorded at various depths in the borehole includes two spikes, and the acceleration recorded at the ground surface is a single spike with amplitude twice as large as the original input signal. If we deconvolve the signal at each depth using the signal from the bottom of the borehole, we obtain waveforms shown in the right portion of Figure 2. In this figure, the input delta function continues reflecting between the ground surface and bottom of the borehole with intrinsic attenuation. The deconvolved wave field is not subject to the boundary condition at the bottom of the borehole, and its decay with time depends on the damping in the soil only [Snieder and Safak, 2006, @].

3.2. Waveform Simulation

The simulated ground motions were computed using the program SHAKE91 [Schnabel et al., 1972, @], which calculates the response for horizontally layered sites [EERC Library in University of California Berkeley, 2005, @]. The input ground motion at the bottom layer is Gaussian white noise high-pass filtered at 20 Hz (see Figure 3). The maximum amplitude of the noise is 10 cm/s^2. The shear strain for this ground motion is less than 0.001%, so the soil response has very little non-linear effect. Theoretically, the deconvolved waveform is an impulse response for a source at the bottom of the borehole. However, if we use a delta function as input, the response includes very high frequency oscillations caused by the Gibbs phenomenon [Gibbs, 1899, @]. In order to more easily calculate the waveforms, we select random Gaussian white noise as the input signal, which can generate a response for a wide frequency range. The Gaussian white noise is assigned as the input motion at the depth of the borehole seismometer for each station, and the response at the ground surface and the bottom of the borehole (input and reflected ground motions) are computed. The simulated surface and borehole waveforms are deconvolved by the same procedure as described in the previous subsection.

At each site, we use the velocity model structure provided by KiK-net [KiK-net, 2000, @]. The density of the soil is not given and assumed to be 2400 kgf/m^3 for all layers. The soil model was represented by horizontal layers with dynamic soil properties (stiffness and damping) as specified in SHAKE91 (see Figure 4) [Seed and Idriss, 1970, @; Idriss, 1990, @]. The soft layers (first or second subsurface layers) in the velocity structure are modeled by the soil properties for sand, and rest of the layers of relatively hard soil are modeled by the properties for rock.

4. Observed and Simulated waveforms for Small Amplitude Shaking

We compared deconvolved waveforms computed from the observed acceleration records with small amplitudes to waveforms computed from the simulated ground motions.

The deconvolved waveforms of the observed acceleration records are obtained as follows; we use deconvolutions for the records of earthquakes before the 2008 Iwate-Miyagi Nairiku earthquake with borehole PGA less than 10 cm/s^2. The sampling of the deconvolved waveform is converted to 200 Hz with a third order Lagrange interpolation for the records with sampling 100 Hz. The amplitude is normalized to one. We stack all available deconvolved waveforms at the same station for the three components.

Figure 1 shows the observed and calculated deconvolved waveforms of the horizontal (EW) component for each station. The black lines show the observed waveforms and the red lines show the results of the simulations. The largest peak is the direct S-wave arrival traveling upward. The later phases are reflected waves from the near-surface structure. The peaks in the waveforms at times before the large initial arrival correspond to the waves traveling from the surface to the bottom. The timing of the observed and simulated waveforms for the direct S-wave agree very well. However, the later phases have some discrepancy in amplitude and frequency. For example, the amplitudes of the observed waveforms at stations IWTH20 and IWTH26 are larger than those of simulated waveforms. There may be many reasons for these discrepancies, but one is the reflection coefficient at the layer boundaries. SHAKE91 assumes vertical incident angle to the boundary. The reflection coefficient is a function of the incident angle, so if the wave is not traveling vertically, the amplitude of the reflected waves is changed. Also, the simulated waveform does not include surface waves which can contaminate the amplitude and frequency of the later phases. We also have some uncertainty of the soil structure in the velocity profile and damping for the simulation. These factors cause the discrepancy between the observed and simulated deconvolved waveforms.

Figure 5 shows the deconvolved waveforms of three stations with typical soil structures. We categorize soil structures into two groups; structure with large velocity contrasts, and the structure with small velocity contrasts. The velocity structure at station AKTH19 has very small velocity contrasts, so the reflection coefficient at the layer boundary is very small. This type of velocity structure generates a pulse-like deconvolved waveform with small later phases. The velocity structure at station IWTH22 has more layers with large velocity contrasts between the layers, which makes the later phases of the deconvolved waveform large and complicated. Station IWTH25 recorded over 4000 cm/s^2 PGA at the ground surface during the 2008 Iwate-Miyagi Nairiku earthquake. The S-wave velocity profile has a large contrast deeper than 100 m, but the velocity contrast in the deep layer produces the long-period waveforms. Therefore, the waveform around the first S-wave arrival is quite simple.

Overall, the deconvolved waveforms of the simulation shown in this section resemble each other and match the observed data reasonable well. This indicates that the velocity structure of the subsurface layers from KiK-net can be used to model the waveforms quite well for small amplitude motions.

5. Nonlinear Effect during Strong Shaking

Figures 6 and 7 show the deconvolved waveforms for earthquakes between July 2001 and December 2008 ordered in time. Figures 6 shows deconvolved waveforms with a duration of 1 s for the EW component, and Figure 7 shows that of UD component. Before the Iwate-Miyagi Nairiku earthquake, the deconvolved accelerograms are very stable and the peaks of the waveforms are almost identical. This peak corresponds to the travel time of the direct P-wave (on the UD component) and S-wave (on EW and NS components) from the bottom of the borehole to the ground surface. However, the S-wave travel time significantly increased for the records of the 2008 Iwate-Miyagi Nairiku earthquake, and the average travel time for aftershocks becomes longer than that of earthquakes before the mainshock. Moreover, the scatter in the shapes of the waveforms and the average travel times for aftershocks are larger than those before the mainshock. These changes indicate that the large amplitude of the ground motion caused strong non-linear changes of the surface soil structure [e.g. Field et al., 1997, @; Hartzell, 1998, @], with a decrease in the velocity.

The incident angle of the ground motion can also affect the estimated travel time. Before the mainshock, most of the events are deep subduction earthquakes and incident angles are close to vertical. However, many of the events after the mainshock are aftershocks that occurred close to the station. These shallow crustal events with larger incident angles, have more contamination from other phases. Also, note that for these close events with larger incidence angles, the apparent vertical travel times would be faster, which is opposite of the observed trend. Therefore, this cannot explain the observed temporal change.

The relationship between the travel time of the peak of the deconvolved waveforms and the values of PGA at the bottom of the borehole is shown in Figure 8 for station IWTH25. The theoretical P- and S-wave travel times computed from the soil data measured in the borehole are also added in the Figure as horizontal lines, which shows the peaks of the NS and EW components correspond to the S-wave travel time, and the peak of vertical component corresponds to the P-wave travel time. Moreover, the travel time increases as a function of the amplitude of the ground motion (PGA). This increase of the travel time (i.e. reduction of the average S-wave velocity) represents the non-linear effect of the surface soil. The reduction of the average P- and S-wave velocities is estimated to be 20% and 24% during the mainshock, respectively, for the 1448 cm/s^2 shaking at IWTH25. Many aftershocks with smaller accelerations that occurred after the mainshock show small or no change in velocity. This indicates that the large velocity changes observed during the mainshock were mostly quickly recovered.

The non-linearization during the strong shaking can be observed at other stations that recorded high accelerations. Figure 9 shows travel times for the station IWTH10, which had only small accelerations and does not show any changes as a function of PGA. Figure 10 shows the travel times for the three components at station IWTH04, which is another example of strong non-linear effects during the strong shaking. The largest PGA at this station was recorded during the 2003 off Miyagi earthquake (M_w 7.0). The reduction of the average P- and S-wave velocities is 11% and 22% during the largest event, respectively. The velocity reduction of IWTH04 for a PGA 217 cm/s^2 is larger than that of IWTH25 at the same level of acceleration, because the depth of the borehole accelerometer is 106 m, which is less than half of that of IWTH25 (260 m). This indicates that the reduction of the velocity probably varies with depth, and is more localized close to the surface.

How much does this velocity reduction change the soil property? The stiffness of the soil G can be expressed as the product of the density ρ and the square of the shear wave velocity V_s ($G = \rho V_s^2$).

Since the velocity reduction is localized near the surface, we assume the stiffness reduction occurs within the 34 m sedimentary deposits close to the surface at station IWTH25. Assuming the soil density is almost constant during the strong shaking, the stiffness reduction can be as large as 78%. We simulated this strong motion record with the velocity structure at the station IWTH25 by SHAKE91. The output shows the stiffness reduction is at most 85% in the sedimentary layer. These numbers are also consistent with the result of Pavlenko and Irikura, 2006 [@], which shows that the shear modulus reduction can be 50-60% and more for the shaking of M_w 6.7-6.8 crustal earthquakes.

6. Static Velocity Reduction

Strong shaking changes the P- and S-wave velocity not only during the strong shaking, but also causes a near-permanent change in the average P- and S-wave velocity. Brenguier et al., 2008 [@] found the velocity reduction and its recovery after the San Simeon and Parkfield earthquakes by using a cross correlation method. They observed the Rayleigh wave velocity reduction between two stations separated by 5 km. The result shows the clear offset during the mainshock and the velocity recovers exponentially after the event. Arai, 2006 [@] also found the recovery process of S-wave velocity of subsurface soils by inversion of microtremor H/V spectra. Here we apply the deconvolution technique to the strong motion records to examine the P- and S-wave travel times before and after the Iwate-Miyagi Nairiku earthquake.

In Figure 8, the average travel time appears to be different before and after the mainshock, with longer travel times after the mainshock. Figure 11 compares the average deconvolved waveforms before and after the 2008 Iwate-Miyagi Nairiku earthquake. The solid thick line is the deconvolved waveform of the mainshock. Although the sampling is not small enough to accurately capture the velocity reduction, the travel time is about 4% longer after the mainshock compared to before. Figure 12 shows a histogram of the travel times before and after the 2008 Iwate-Miyagi Nairiku earthquake. Standard deviations of the travel times are small, which means the average velocity is stable in time and event.

Therefore, there is a clear shift toward longer travel times (P and S wave velocity reductions) after the 2008 Iwate-Miyagi Nairiku earthquake.

In general, strong excitation causes non-linear effects in the soil during the shaking, but it usually quickly recovers after the shaking. However, this significantly large acceleration changed the soil property and the soil did not fully recover after the shaking. This velocity reduction might be expected to recover exponentially in the long term [Brenguier et al., 2008, @; Sawazaki et al., 2009, @]. Figure 13 shows the temporal change of the S-wave travel time for the station IWTH25. The records with borehole PGA less than 10 cm/s^2 are used for this plot. Since the data include some unreasonably short and long travel times (see Figure 12), for the average values shown in Figure 13, we limit the data to travel times between 2.4 and 3.0 s. The velocity reduction caused by the strong shaking recovers as a function of the logarithm of the lapse time, but has not yet completely returned in one year.

Such a large static offset of the average velocity due to the strong shaking is not observed in other stations, since the acceleration is not as large as that of IWTH25. Because we focus on the travel time for distances of 100 - 200 m, the amplitude of the velocity reduction is quite small. Either extending the distance or using higher sampling data may be able to detect velocity changes associated with smaller ground motions.

7. Conclusions

In this paper, we apply a deconvolution method to strong motion data recorded at the ground surface and at depth in boreholes, and try to characterize the nonlinear effect of the near-surface soils during strong shaking.

The deconvolved waveforms reflect the subsurface velocity structure, and their horizontal and vertical components correspond to S- and P-wave, respectively, traveling from the downhole sensor to the surface. When the accelerations of the borehole records are small, nonlinear effects are not significant and the deconvolved waveforms of the observation can be simulated well using SHAKE91.

During the 2008 Iwate-Miyagi Nairiku earthquake, the strong high-frequency motions caused non-linear changes of the soil in the near-source region, with a reduction of the average shear wave velocity of 24%. The stiffness reduction localized at the subsurface can be 70-80% according to the SHAKE91 simulation. This significantly strong shaking changed the soil property and the stiffness coefficient did not fully recover after the shaking, leaving a static change.

Acknowledgments.
The authors acknowledge the National Research Institute for Earth Science and Disaster Prevention (NIED) for the use of strong motion data. The SHAKE91 program is provided by UC Berkeley. We appreciate the advice from Dr. Takao Kagawa in Tottori University for the soil response analysis. We are deeply appreciative of comments provided by the associate editor and reviewers.

This research was supported by the Program for Improvement of Research Environment for Young Researchers from Special Coordination Funds for Promoting Science and Technology (SCF) commissioned by the Ministry of Education, Culture, Sports, Science and Technology (MEXT) of Japan.

References

Arai, H. (2006). Detection of Subsurface vs Recovery Process Using Microtremor and Weak Ground Motion Records in Ojiya, Japan. *Proceedings of the 3rd International Conference on Urban Earthquake Engineering,* Tokyo Institute of Technology, Tokyo, Japan:631–638.

Brenguier, F., Campillo, M., Hadziioannou, C., Shapiro, N., Nadeau, R., and Larose, E. (2008). Postseismic Relaxation along the San Andreas Fault at Parkfield from Continuous Seismological Observations. *Science*, 321(5895):1478.

Clayton, R. and Wiggins, R. (1976). Source Shape Estimation and Deconvolution of Teleseismic Body Waves. *Geophys. J. R. Astron. Soc.*, 47:151–177.

EERC Library in University of California Berkeley (2005). SHAKE-91 software and manuals, http://nisee.berkeley.edu/elibrary/.

Field, E., Johnson, P., Beresnev, I., and Zeng, Y. (1997). Nonlinear Ground-motion Amplification by Sediments during the 1994 Northridge Earthquake. *Nature*, 390(6660):599–602.

Gibbs, J. (1899). Fourier series. *Nature*, 59(1522):200.

Hartzell, S. (1998). Variability in Nonlinear Sediment Response during the 1994 Northridge, California, Earthquake. *Bull. Seismol. Soc. Am.*, 88(6):1426–1437.

Idriss, I. (1990). Response of Soft Soil Sites during Earthquakes. *Proceedings, H Bolton Seed Memorial Symposium*, 273–289.

KiK-net (2000). http://www.kik.bosai.go.jp/kik/index_en.shtml.

Kohler, M., Heaton, T., and Bradford, S. (2007). Propagating Waves in the Steel, Moment-frame Factor Building Recorded during Earthquakes. *Bull. Seismol. Soc. Am.*, 97:1334–1345.

Mehta, K., Snieder, R., and Graizer, V. (2007). Downhole Receiver Function: A Case Study. *Bull. Seismol. Soc. Am.*, 97(5):1396–1403.

Miyazawa, M., Snieder, R., and Venkataraman, A. (2008). Application of Seismic Interferometry to Extract P-and S-wave Propagation and Observation of Shear-wave Splitting from Noise Data at Cold Lake, Alberta, Canada. *Geophysics*, 73(4):D35–D40.

Pavlenko, O. and Irikura, K. (2006). Nonlinear Behavior of Soils Revealed from the Records of the 2000 Tottori, Japan, Earthquake at Stations of the Digital Strong-motion Network KiK-net. *Bull. Seismol. Soc. Am.*, 96(6):2131–2145.

Sabra, K., Gerstoft, P., Roux, P., Kuperman, W., and Fehler, M. (2005). Extracting Time-domain Green's Function Estimates from Ambient Seismic Noise. *Geophys. Res. Let.*, 32:L03310.

Sawazaki, K, Sato, H, Nakahara, H, and Nishimura, T. (2009). Time-Lapse Changes of Seismic Velocity in the Shallow Ground Caused by Strong Ground Motion Shock of the 2000 Western-Tottori Earthquake, Japan, as Revealed from Coda Deconvolution Analysis. *Bull. Seismol. Soc. Am.*, 99(1):352–366.

Schnabel, P., Lysmer, J., and Seed, H. (1972). SHAKE: A Computer Program for Earthquake Response Analysis on Horizontally Layered Sites. *Earthquake Engineering Research Center, University of California, Berkeley*, report no. EERC 72-12.

Seed, H. and Idriss, I. (1970). Soil Moduli and Damping Factors for Dynamic Response Analysis. *Earthquake Engineering Research Center, University of California, Berkeley*, report no. EERC 70-10.

Snieder, R. (2004). Extracting the Green's Function from the Correlation of Coda Waves: A Derivation Based on Stationary Phase. *Physical Review E, Statistical Physics, Plasmas, Fluids, and Related Interdisciplinary Topics*, 69(4).

Snieder, R. and Safak, E. (2006). Extracting the Building Response Using Seismic Interferometry: Theory and Application to the Millikan Library in Pasadena, California. *Bull. Seismol. Soc. Am.*, 96(2):586–598.

Vasconcelos, I. and Snieder, R. (2008a). Interferometry by Deconvolution, Part 1 - Theory for Acoustic Waves and Numerical Examples. *Geophysics*, 73:S115.

Vasconcelos, I. and Snieder, R. (2008b). Interferometry by Deconvolution: Part 2 - Theory for Elastic Waves and Application to Drill-bit Seismic Imaging. *Geophysics*, 73:S129.

M. Yamada, Kyoto University, Uji, Gokasho, 611-0011, Japan (masumi@eqh.dpri.kyoto-u.ac.jp)

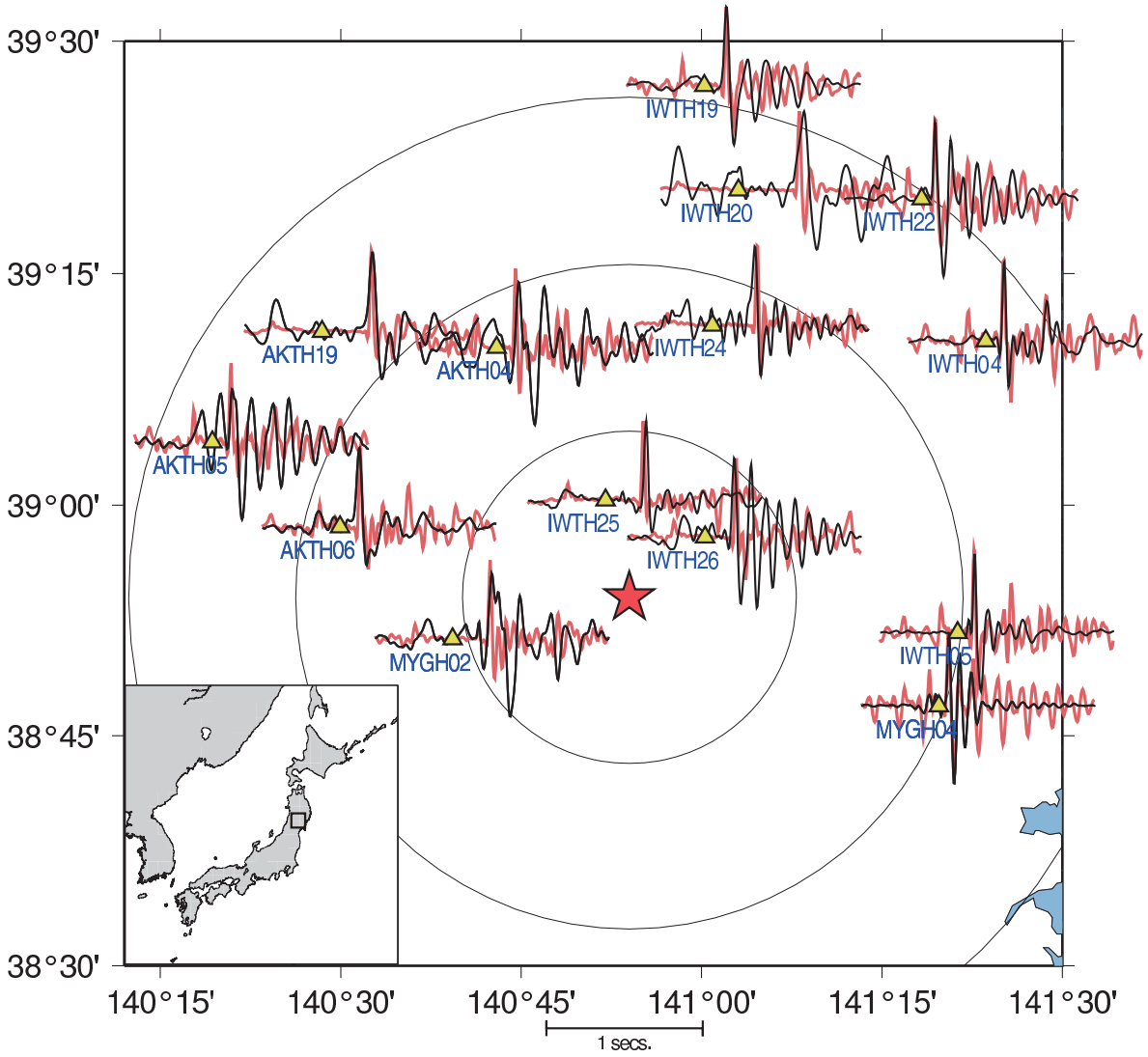

Figure 1. Average deconvolved waveforms for the EW component of KiK-Net stations in northeast Honshu. The black lines show the deconvolved waveforms for the acceleration records with small amplitudes. The red lines show the waveforms from the simulation with SHAKE91. The yellow triangles show the location of the stations and origin of the time axis on the waveforms. A star shows the epicenter of the 2008 Iwate-Miyagi Nairiku earthquake. The areas within 20, 40, and 60 km from the epicenter are shown by large circles.

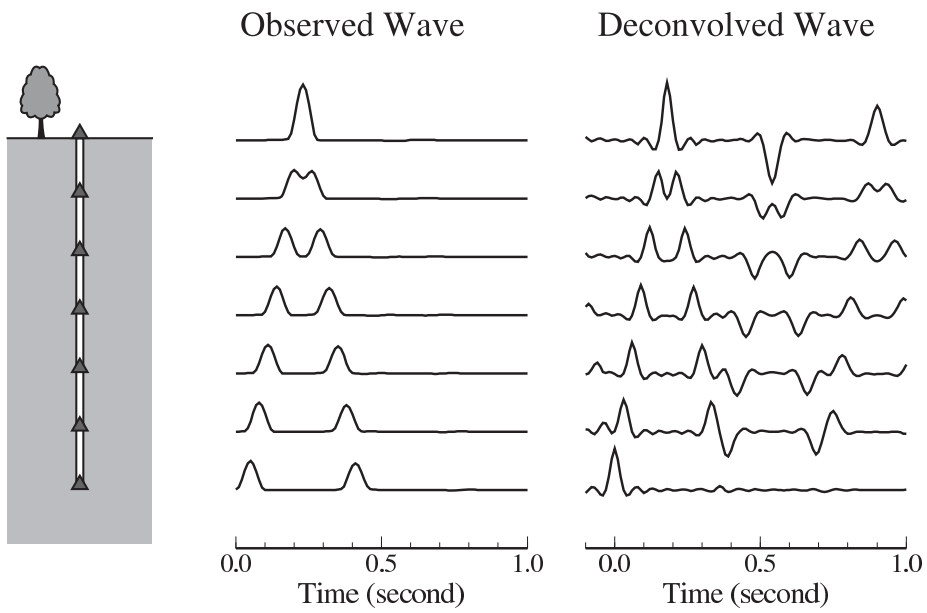

Figure 2. The calculated waveforms and deconvolved waveforms for a delta function input at the bottom of the borehole.

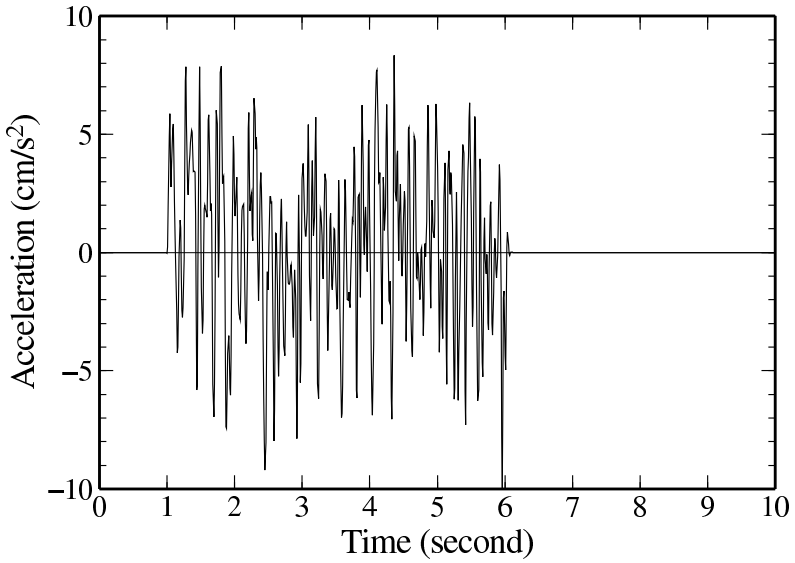

Figure 3. Gaussian noise used as an input motion for the ground motion simulation by SHAKE91.

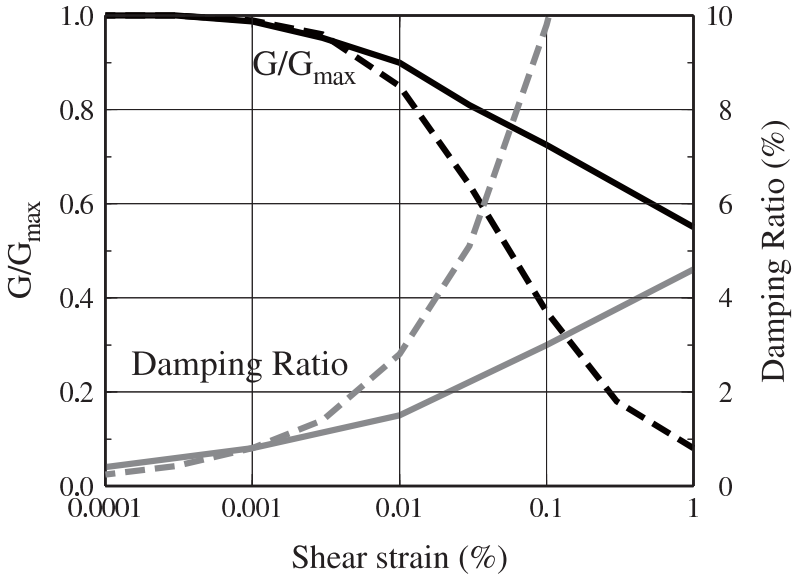

Figure 4. Modulus reduction (black lines) and damping change (gray lines) used for the simulation by SHAKE91. The solid lines are the properties for rock, and the dashed lines are for sand.

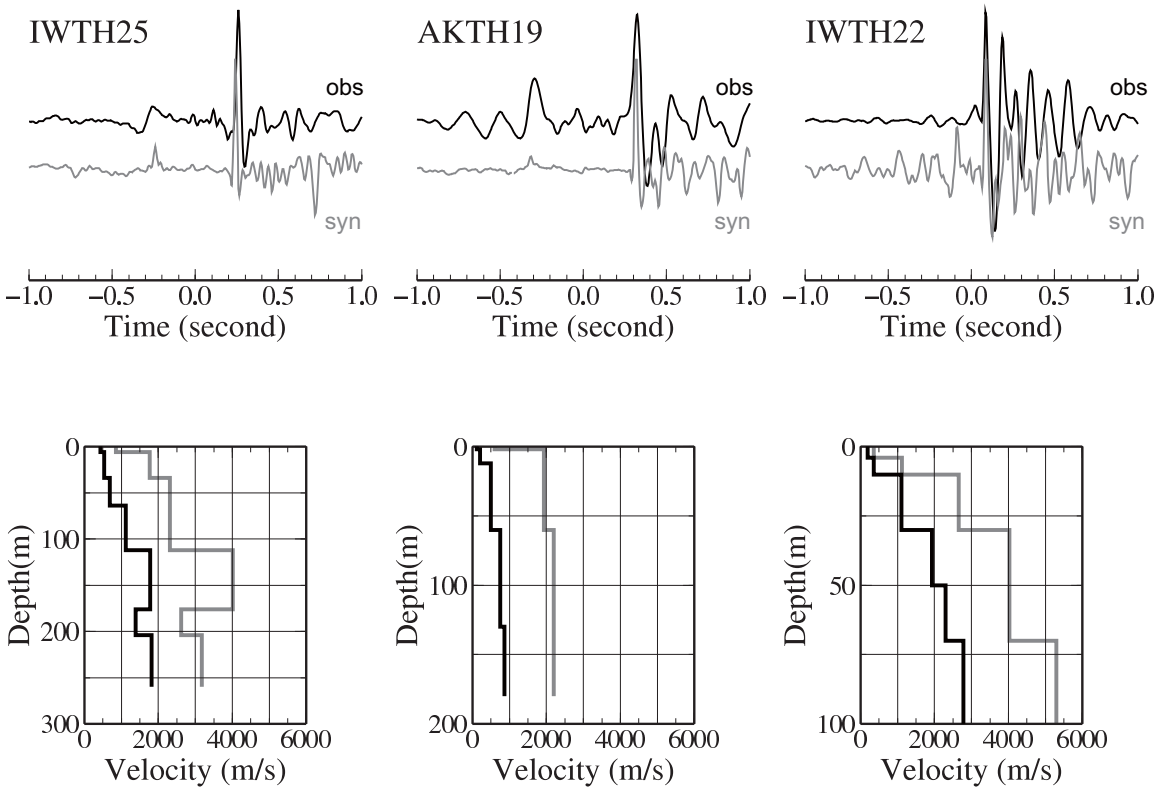

Figure 5. Deconvolved waveforms for the EW component and velocity structure for the stations IWTH25, AKTH19, and IWTH22. Top figure: The black lines show the deconvolved waveforms for the observed acceleration records with small amplitudes. The gray lines show the deconvolved waveforms from the simulation with SHAKE91. Bottom figure: gray and black lines are P- and S-wave velocity structure, respectively, used for the simulation.

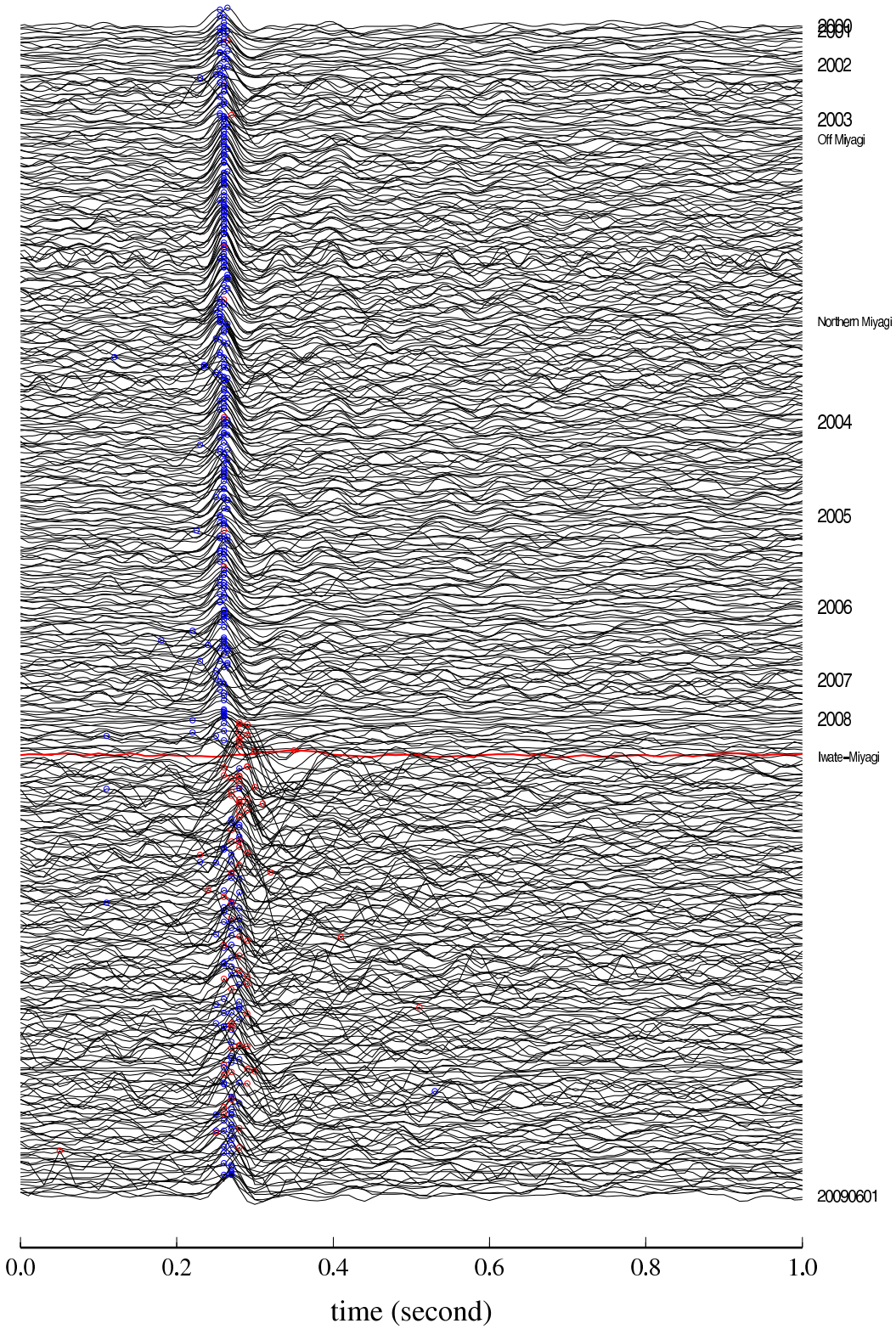

Figure 6. Deconvolved accelerograms of EW component for station IWTH25 ordered in time. Note that the time scale in the vertical direction is not linear, as shown in the right side. The red curve is the Iwate-Miyagi Nairiku earthquake. The red and blue circles indicate the peak of each deconvolved function for the records with borehole PGA greater or equal to, and less than, 10 cm/s^2, respectively. The vertical scale is identical for all waveforms.

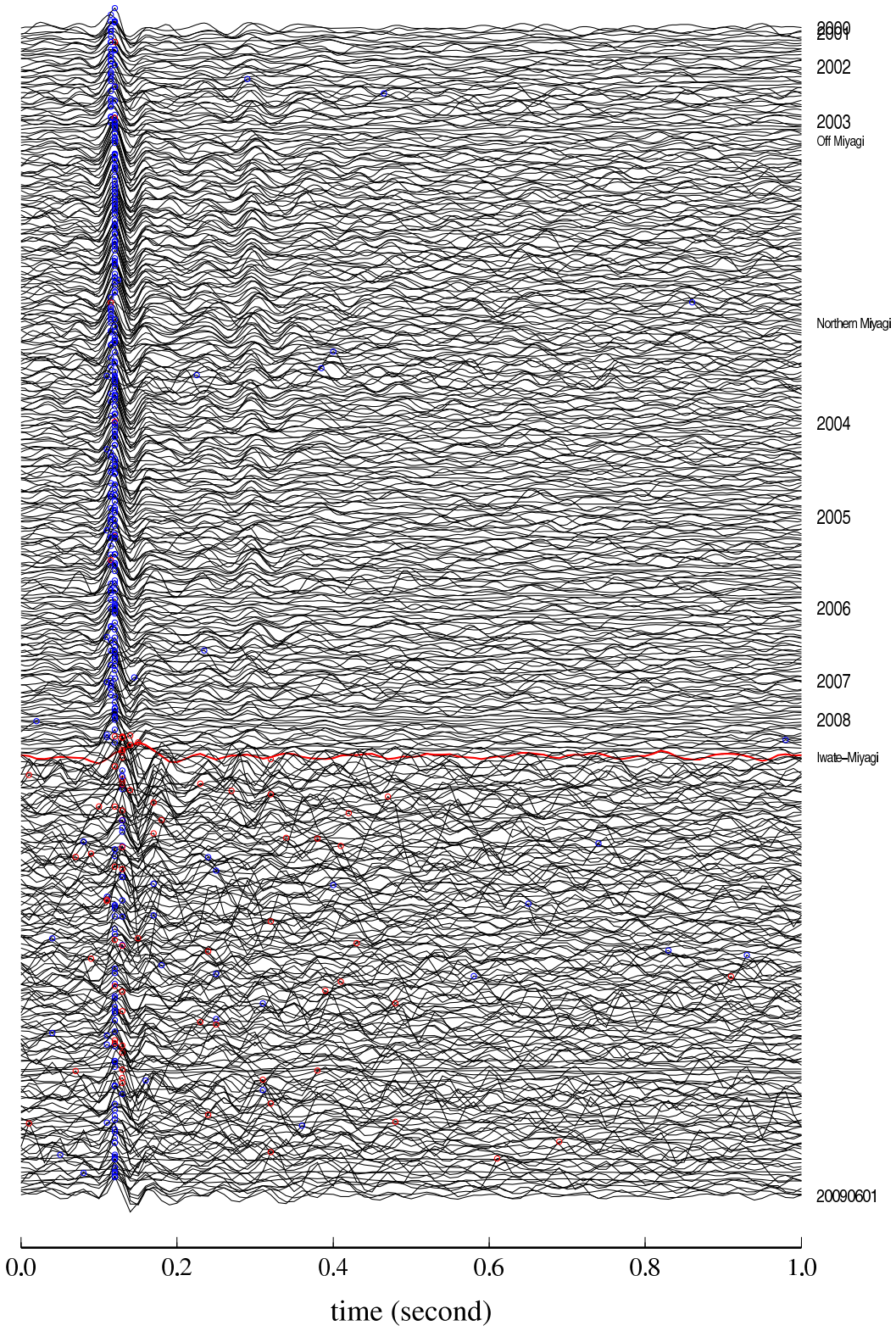

Figure 7. Deconvolved accelerograms of the UD component for station IWTH25 ordered in time. The symbols are the same as Figure 6.

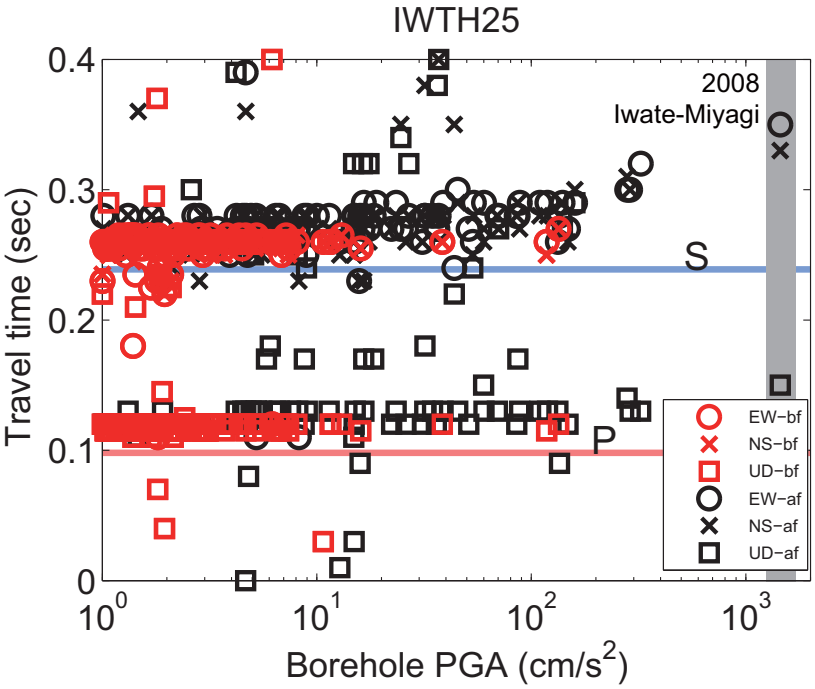

Figure 8. Travel times from borehole sensor to surface sensor as a function of PGA for station IWTH25. The red and black symbols are events before and after the largest event (2008 Iwate-Miyagi Nairiku earthquake), respectively. The red and blue horizontal lines show the theoretical P- and S-wave travel times from the site data measured in the borehole.

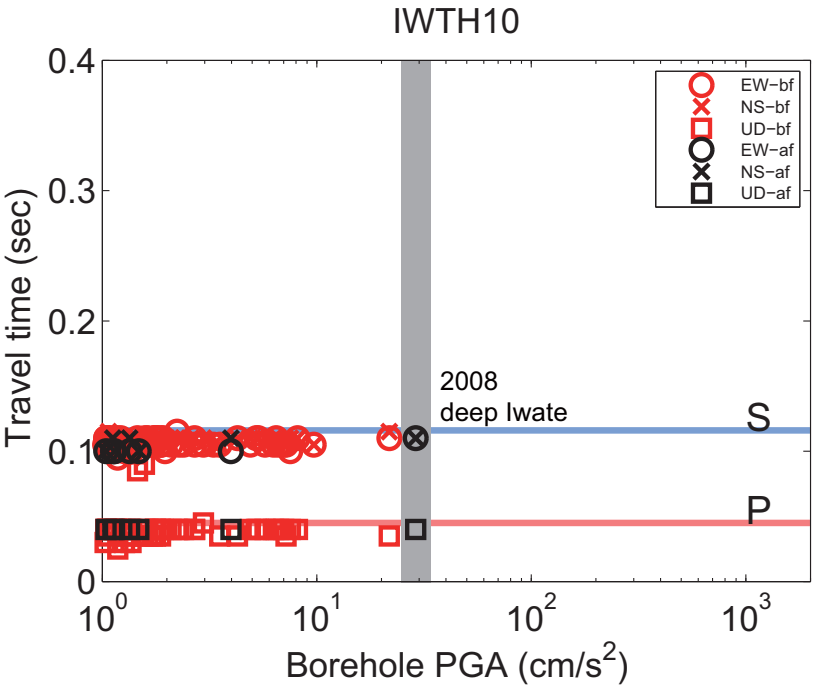

Figure 9. Travel times from borehole sensor to surface sensor as a function of PGA for station IWTH10. The red and black symbols are events before and after the largest event (2008 Deep Iwate earthquake), respectively. The symbols are the same as Figure 8.

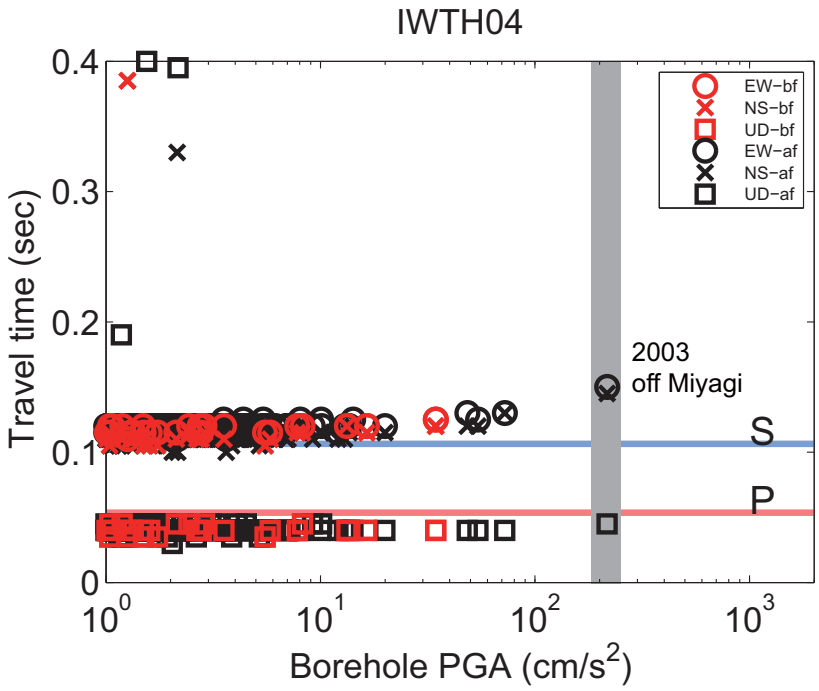

Figure 10. Travel times from borehole sensor to surface sensor as a function of PGA for station IWTH04. The red and black symbols are events before and after the largest event (2003 off Miyagi earthquake), respectively. The symbols are the same as Figure 8.

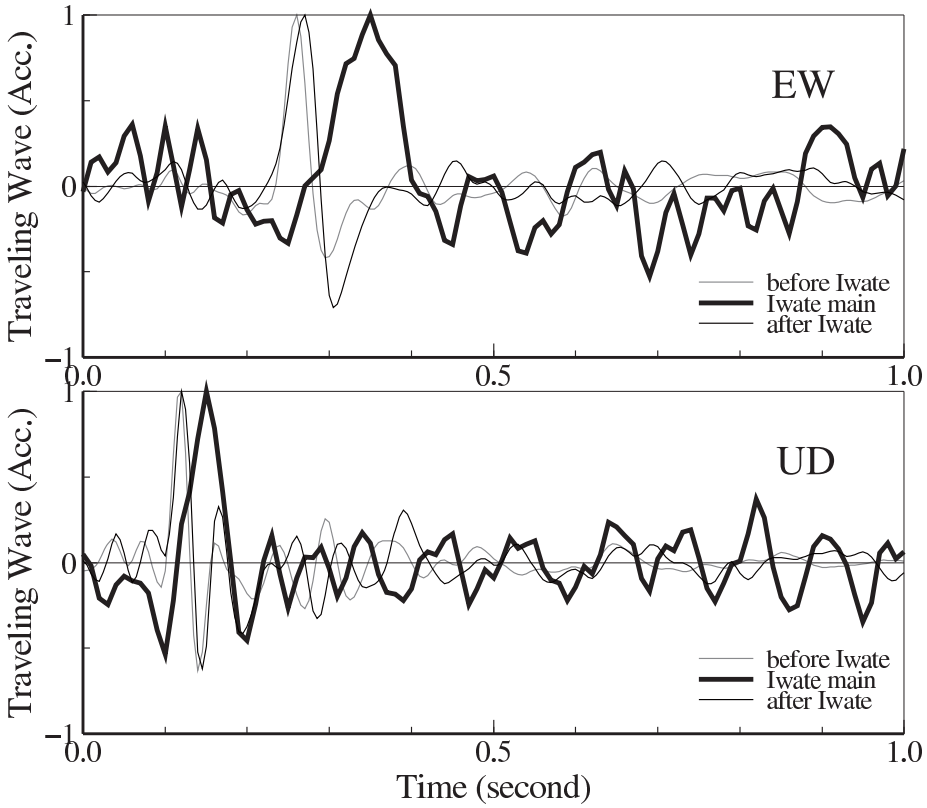

Figure 11. Deconvolved waveforms for the station IWTH25. The gray and black line show the waveforms of the stacked records with small PGA for events before and after the 2008 Iwate-Miyagi Nairiku earthquake, respectively. The solid thick line is the deconvolved waveform of the mainshock.

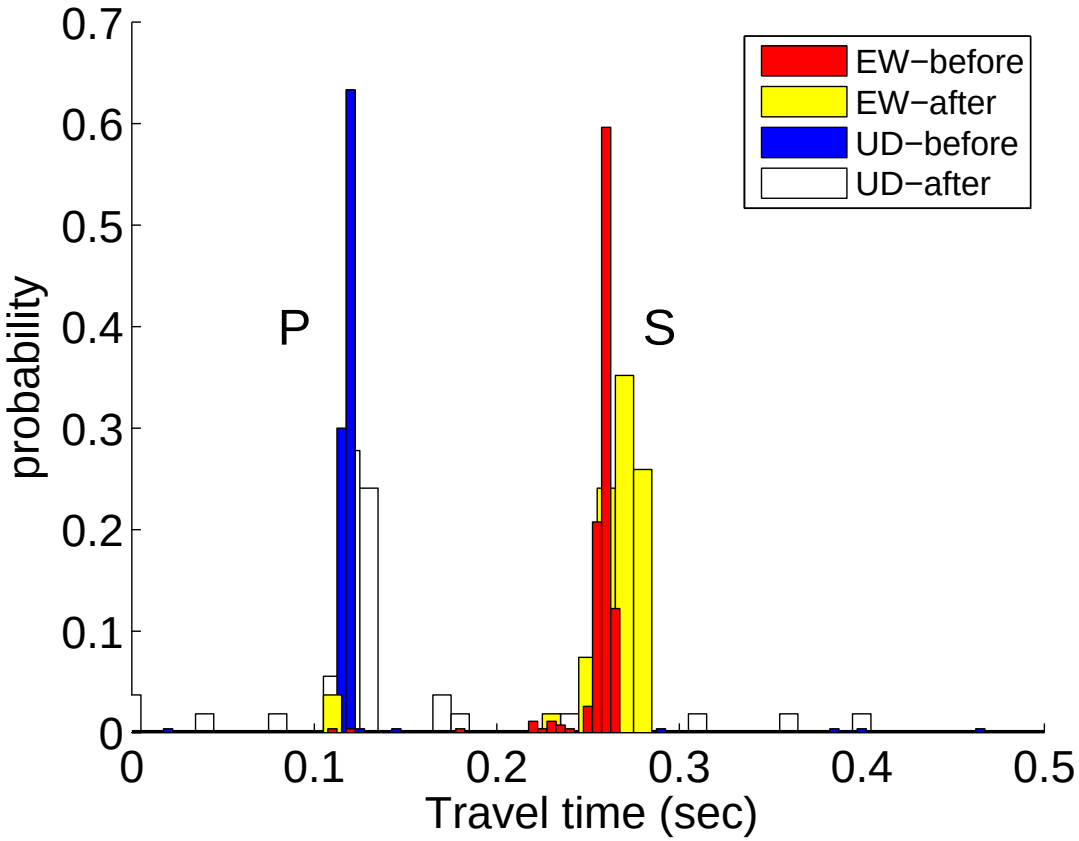

Figure 12. Histogram of travel times from the downhole sensor to the surface sensor for station IWTH25. The bin height is normalized by the total number of records in each category so that the sum of bin heights is 1. The red and blue bars show the travel times for events before the 2008 Iwate-Miyagi Nairiku earthquake, and yellow and white bars show the travel times for events after the 2008 Iwate-Miyagi Nairiku earthquake, respectively. The different bin widths reflect the change of the sampling (200Hz and 100Hz).

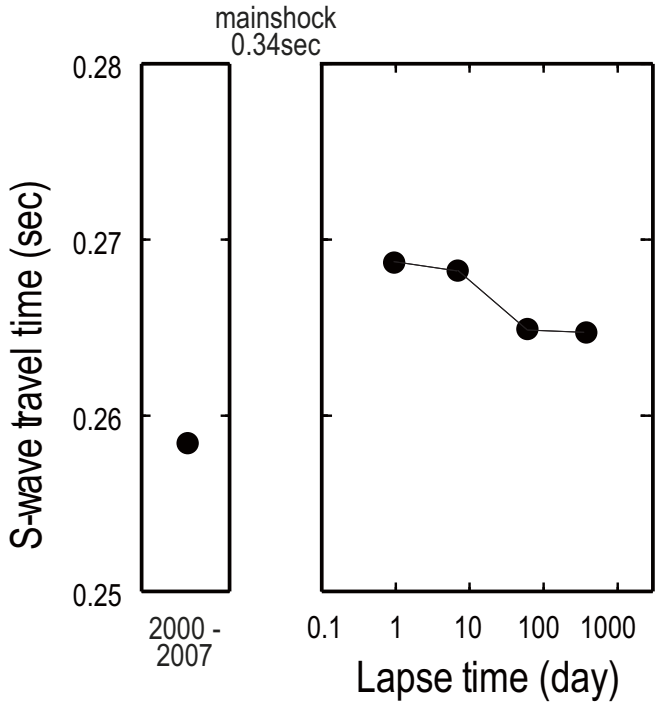

Figure 13. Temporal change of the S-wave travel time before and after the mainshock for the station IWTH25. The travel time is computed from the avarage of EW and NS components. Left box shows the average travel time between 2000 and 2007, and the right box shows the average travel time after the 2008 Iwate-Miyagi Nairiku earthquake. The four points in the right box are for average values of 0 to 1 day, 1 day to 1 week, 1 week to 2 months and 2 month to 1 year, after the mainshock.